Arabian Journal for Science and Engineering (2018) 43:4703–4712
https://doi.org/10.1007/s13369-017-3038-5

RESEARCH ARTICLE - MECHANICAL ENGINEERING

Mapping the Efficiency of the Hydrostatic Drive for the Rotary Head of Drill Machine Using High-Speed Low-Torque Hydraulic Motors

Alok Vardhan[1] · **K. Dasgupta**[1]

Received: 10 April 2017 / Accepted: 20 December 2017 / Published online: 18 January 2018

Abstract
A method for producing the efficiency map of the hydrostatic drive used in the rotary head of drill machine is discussed in this article. Such map may be useful for the initial assessment of the drive efficiency. In a drill machine used in open-cast mining application, the drill bit is rotated by a hydrostatic drive, which consists of a variable displacement pump and two fixed displacement hydraulic motors along with a gear reducer unit. In this respect, performance investigation of such drive is carried out through mathematical modelling and experimentation. The results are presented in non-dimensional form for selecting a transmission of any size. On the basis of results obtained, the best efficient zone of the proposed hydrostatic drive with respect to the load torque and the drive speed for the rotary head of drill machine is also discussed.

Keywords Hydrostatic (HST) drive · Continuously variable transmission (CVT) · Efficiency map · Pump · Hydraulic motor

List of symbols

D_p	Volumetric displacement of the pump (m^3/rad)
D_{pmax}	Maximum volumetric displacement of the pump (m^3/rad)
D_m	Fixed volumetric displacement of the hydraulic motor (m^3/rad)
P	Fluid pressure on the high-pressure side of the drive (N/m^2)
Q_m	Total volumetric flow rate from the motors (m^3/s)
Q_p	Volumetric flow rate on the discharge side of the pump (m^3/s)
Q_{lm}	Leakage flow of the motor (m^3/s)
Q_{lp}	Leakage flow of the pump (m^3/s)
R_{el}	External leakage resistance of the motor (Ns/m^5)
R_{il}	Internal leakage resistance of the motor (Ns/m^5)
R_{pd}	Drag resistance of the pump (Nsm)
R_{pl}	Leakage resistance of the pump (Ns/m^5)
T_d	Torque on the drive shaft (Nm)
T_m	Torque on the output shaft of the each hydraulic motor (Nm)
T_p	Torque on the input shaft of the pump (Nm)
$\overline{\alpha}$	Normalized swash plate angle of the pump
ΔT_{loss}	Torque loss of the each hydraulic motor (Nm)
η_g	Efficiency of the gear unit
η_m	Efficiency of the hydraulic motor
η_o	Overall efficiency of the HST drive
η_p	Efficiency of the pump
ω_d	Angular velocity of the drive shaft (rad/s)
ω_m	Angular velocity of the motor shaft (rad/s)
ω_p	Angular velocity of the pump shaft (rad/s)

✉ Alok Vardhan
alok.or.monu@gmail.com

[1] Department of Mining Machinery Engineering, Indian Institute of Technology (Indian School of Mines), Dhanbad, Dhanbad, Jharkhand 826004, India

1 Introduction

In understanding the topographical behaviour of the machineries, efficiency maps are widely used by the application engineers. Such maps are generated usually for the prime movers where the torque speed characteristics of them with respect to the variation of fuel supply (in case of internal combustion engine) are shown. From such maps, the engineers are able to determine the operating zone of the prime mover within reasonable efficiency for the desired output power. An HST drive is a continuously variable transmission (CVT) by which the torque and speed can be varied within wide range without the need of gear unit. They are used to propel the heavy earth moving machinery used in construction and mining industries. Considerable literature are available for the HST drive and its components. However, very limited

literature are available regarding the efficiency map of the HST drive.

Manring [1] has proposed a method to generate efficiency map for the HST drive and has presented a typical set of maps that may be useful for the initial design of the machineries where such drive is used. Efficiency map for a linear hydraulic actuator has also proposed by Manring [2] and depicted that the proposed actuator is operated below a wide-open valve line that has the efficiencies less than 50%. Wang et al. [3] have presented the pump and motor models where, based on the parameter optimization algorithm, nonlinear characteristics of the losses are considered. Vanwalleghem et al. [4] have investigated the optimization of the efficiency of hydrostatic drives and proposed a procedure for the speed control of such drive train and also validated this drive train on a 110 kW test bench. Vardhan et al. [5] have proposed two closed-circuit HST drives for the rotary head of drill machine. From the study, they concluded that the low-speed high-torque hydrostatic drive is suitable for slower penetration rate because it gives better efficiency for operating at lower span of speed. In contrast, the high-speed low-torque drive is ideal for faster penetration rate because it gives better efficiency at higher span of speed. Comellas et al. [6] have worked on modelling and study of driveline with hydrostatic transmission system of all-terrain vehicles (ATV). They have presented a methodology for study of hydrostatic transmission system and procedure to describe mathematical modelling of each component before developing a global model for whole driveline.

In a drill machine, the drill bit is rotated by a continuously variable hydrostatic drive, which consists of a variable displacement pump and two fixed displacement high-speed low-torque motors along with a gear reducer unit [7]. A schematic representation of the drive arrangement for the rotary head of a drill machine is shown in Fig. 1. The speed of the drill bit rotated by fixed displacement hydraulic motors along with a gear reducer unit is controlled by variable flow supplied from a swash plate-controlled variable displacement pump. This article proposes a method for producing the efficiency map of an HST drive for the rotary head of drill machine which may be useful as a first approximation in the assessment of drive's efficiency. The results of this paper are presented in non-dimensional form, so that selection of any size of the HST drive can be made.

2 HST Drive Description

The schematic representation of HST drive for the rotary head of drill machine is given in Fig. 2. A variable displacement pump driven by a prime mover supplies pressurized fluid (Q_p) to the hydraulic motors. In turn, the motors convert the fluid power to mechanical power that drives the drill bit through gear reducer unit. By varying the swash plate angle ($\overline{\alpha}$), the fluid power from the pump to the motors is regulated. In Fig. 2, the high-pressure side has fluid pressure denoted by the symbol P, whereas the pressure of the low-pressure side is considered to be zero.

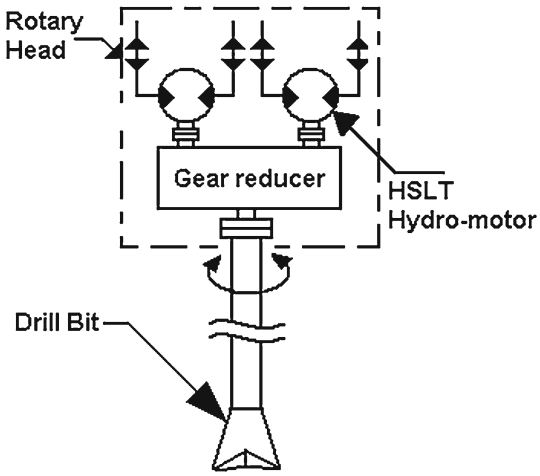

Fig. 1 Drive arrangement for the rotary head system of a drill machine

The analysis have been made based on the above schematic representation. The more detailed diagram is discussed in the experimental test set-up given in "Appendix 1".

The overall efficiency of the HST drive is expressed as:

$$\eta_o = \frac{T_d \omega_d}{T_p \omega_p} \tag{1}$$

where T_p, T_d, ω_p and ω_d are the input torque on the pump shaft, the output torque on the drive shaft, the pump speed and the drive speed, respectively. In terms of pump, motor and gear unit efficiencies, Eq. (1) may also be expressed as:

$$\eta_o = \frac{PQ_p}{T_p \omega_p} \times \frac{2T_m \omega_m}{PQ_p} \times \frac{T_d \omega_d}{2T_m \omega_m} = \eta_p \times \eta_m \times \eta_g \tag{2}$$

where η_p, η_m and η_g are the pump, motor and the gear unit efficiencies, respectively. They are analysed and modelled in Sect. 3 of this article.

3 Analysis and Modelling

3.1 Pump Analysis

The overall efficiency of the pump is given by:

$$\eta_p = \frac{PQ_p}{T_p \omega_p} \tag{3}$$

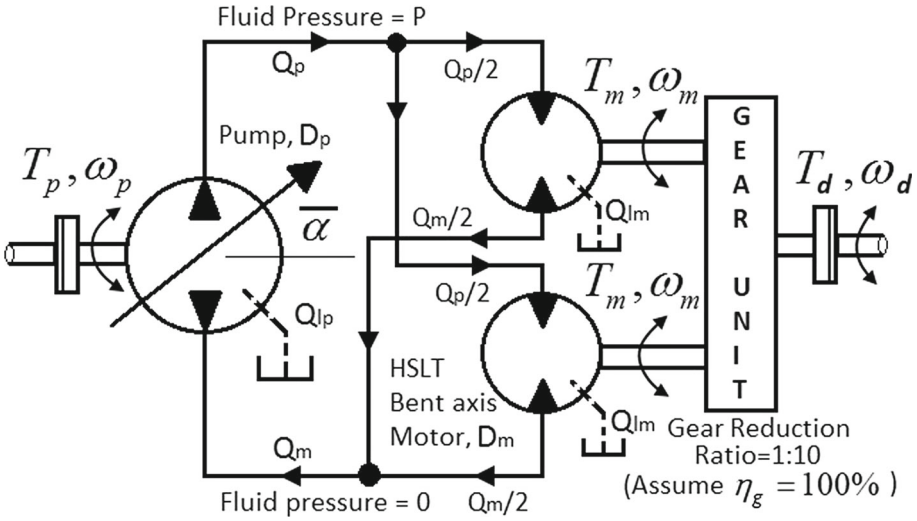

Fig. 2 Schematic of the HST drive

From Fig. 2, the pump supply is given as:

$$Q_{\mathrm{p}} = D_{\mathrm{pmax}}\omega_{\mathrm{p}}\overline{\alpha} - Q_{\mathrm{lp}} \tag{4}$$

where D_{pmax} is the maximum volumetric displacement of the pump, $\overline{\alpha}\left(=\frac{D_{\mathrm{p}}}{D_{\mathrm{pmax}}}\right)$ is the normalized swash plate angle of the pump which ranges from $0 \le \overline{\alpha} \le 1$ and Q_{lp} is the leakage flow of the pump and it is given by:

$$Q_{\mathrm{lp}} = \frac{P}{R_{\mathrm{pl}}} \tag{5}$$

where R_{pl} is the leakage resistance of the pump and it is determined from the test data.

The variation of R_{pl} with $\overline{\alpha}$ shown in Fig. 3 is expressed by the following empirical equation:

$$\begin{aligned} R_{\mathrm{pl}} \times 10^{-11} = {} & \left(10^{-7}P - 0.2318\right)\overline{\alpha}^2 \\ & + \left(-7 \times 10^{-8}P + 1.2568\right)\overline{\alpha} \\ & + \left(-3 \times 10^{-7}P + 7.2137\right) \end{aligned} \tag{6}$$

Substituting Eqs. (5) and (6) into Eq. (4) gives the following expression for the supply flow of the pump:

$$Q_{\mathrm{p}} = D_{\mathrm{pmax}}\omega_{\mathrm{p}}\overline{\alpha} - \frac{P \times 10^{-11}}{\left[\left(10^{-7}P - 0.2318\right)\overline{\alpha}^2 + \left(-7 \times 10^{-8}P + 1.2568\right)\overline{\alpha} + \left(-3 \times 10^{-7}P + 7.2137\right)\right]} \tag{7}$$

The torque input of the pump is a combination of ideal torque and the torque loss due to mechanical efficiency of the pump. It is expressed as:

$$T_{\mathrm{p}} = D_{\mathrm{pmax}}P\overline{\alpha} + \omega_{\mathrm{p}}R_{\mathrm{pd}} \tag{8}$$

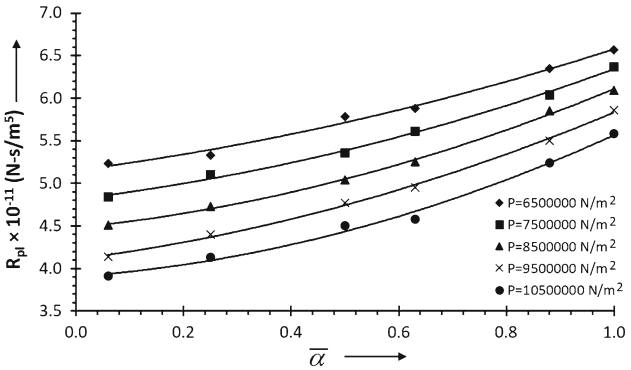

Fig. 3 Leakage resistance characteristics of the pump

where the second term of Eq. (8) represents the ideal torque and the third term is the torque loss due to the drag resistance (R_{pd}) of the pump. The characteristics of the R_{pd} are obtained from the test data.

The variation of R_{pd} with $\overline{\alpha}$ shown in Fig. 4 is expressed by the following empirical equation:

$$R_{\mathrm{pd}} \times 10^2 = \left(-8 \times 10^{-8}P + 0.8659\right)\overline{\alpha} + \left(10^{-7}P - 0.1322\right) \tag{9}$$

Substituting Eq. (9) into Eq. (8) gives the expression for the input torque on the pump shaft:

$$\begin{aligned} T_{\mathrm{p}} = {} & D_{\mathrm{pmax}}P\overline{\alpha} \\ & + \omega_{\mathrm{p}}\left[\frac{\left(-8 \times 10^{-8}P + 0.8659\right)\overline{\alpha} + \left(10^{-7}P - 0.1322\right)}{10^2}\right] \end{aligned} \tag{10}$$

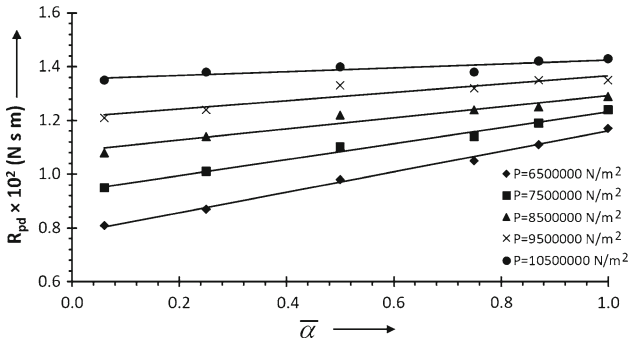

Fig. 4 Drag resistance characteristics of the pump

Equations (3), (7) and (10) are non-dimensionalized using the following relations:

$$Q_p = \overline{Q_p} D_{pmax} \omega_p, \quad P = \overline{P} P_{max}, \quad T_p = \overline{T_p} D_{pmax} P_{max} \tag{11}$$

where symbols with bars are non-dimensional. Substituting them in Eq. (3), the pump efficiency is given by:

$$\eta_p = \frac{\overline{P}\,\overline{Q_p}}{\overline{T_p}} \tag{12}$$

Similarly, using Eq. (11) in Eq. (7), the non-dimensional supply flow of the pump is:

$$\overline{Q_p} = \overline{\alpha} - \frac{K_0 \overline{P}}{\left[\left(K_1 \overline{\alpha}^2 - K_3 \overline{\alpha} - K_5\right)\overline{P} - K_2 \overline{\alpha}^2 + K_4 \overline{\alpha} + K_6\right]} \tag{13}$$

where

$$\begin{aligned} K_0 &= \frac{P_{max}}{D_{pmax}\omega_p}, \; K_1 = 10^4 P_{max}, \\ K_2 &= 0.2318 \times 10^{11}, \; K_3 = 7 \times 10^3 P_{max}, \\ K_4 &= 1.2568 \times 10^{11}, \; K_5 = 3 \times 10^4 P_{max}, \\ K_6 &= 7.2137 \times 10^{11} \end{aligned} \tag{14}$$

Finally, using Eq. (11) in Eq. (10), the non-dimensional representation of the pump torque may be given as:

$$\overline{T_p} = \overline{\alpha}\,\overline{P} + \left(-B_0 \overline{\alpha} + B_2\right)\overline{P} + B_1 \overline{\alpha} - B_3 \tag{15}$$

where

$$\begin{aligned} B_0 &= \frac{8 \times 10^{-10} \omega_p}{D_{pmax}}, \; B_1 = \frac{0.8659 \times 10^{-2} \omega_p}{D_{pmax} P_{max}}, \\ B_2 &= \frac{10^{-9} \omega_p}{D_{pmax}}, \; B_3 = \frac{0.1322 \times 10^{-2} \omega_p}{D_{pmax} P_{max}} \end{aligned} \tag{16}$$

After obtaining the values of the coefficients given in Eqs. (14) and (16), the efficiency map of the pump is generated from the simultaneous solutions of Eqs. (12), (13) and (15). This is discussed in Sect. 4.

3.2 Hydraulic Motor Analysis

The overall efficiency of the hydraulic motor is given by:

$$\eta_m = \frac{2 T_m \omega_m}{P Q_p} \tag{17}$$

The angular velocity of the motor shaft is:

$$\omega_m = \frac{Q_m/2}{D_m} \tag{18}$$

where $Q_m/2$ is the discharge flow from the each motor and D_m is the fixed volumetric displacement rate of the motor.

The discharge flow from the each motor is given by:

$$\frac{Q_m}{2} = \frac{Q_p}{2} - Q_{lm} \tag{19}$$

where, neglecting the line leakage, $Q_p/2$ is the motor inlet flow and Q_{lm} is the leakage flow of the motor that is expressed as:

$$Q_{lm} = \frac{P}{R_{il}} + \frac{P}{R_{el}} \tag{20}$$

where R_{il} and R_{el} are the internal and the external leakage resistances of the hydraulic motor and these are determined from the test data.

The variation of R_{il} and R_{el} with $\overline{\alpha}$ shown in Figs. 5 and 6 is expressed by the following empirical equations:

$$\begin{aligned} R_{il} \times 10^{-12} &= \left(-8 \times 10^{-10} P - 0.0006\right)\overline{\alpha} \\ &\quad + \left(-3 \times 10^{-9} P + 1.1155\right) \end{aligned} \tag{21}$$

$$\begin{aligned} R_{el} \times 10^{-11} &= \left(2 \times 10^{-6} P - 19.182\right)\overline{\alpha} \\ &\quad + \left(-2 \times 10^{-6} P + 25.836\right) \end{aligned} \tag{22}$$

Combining Eqs. (7) and (18) through (20) gives the following expression for the angular speed of the motor output shaft:

$$\omega_m = \frac{1}{2D_m}\left[D_{pmax}\omega_p \overline{\alpha} - \frac{P}{R_{pl}} - \frac{2P}{R_{il}} - \frac{2P}{R_{el}}\right] \tag{23}$$

The torque on the each motor shaft is a combination of ideal torque minus torque loss and it is expressed as:

$$T_m = D_m P - \Delta T_{loss} \tag{24}$$

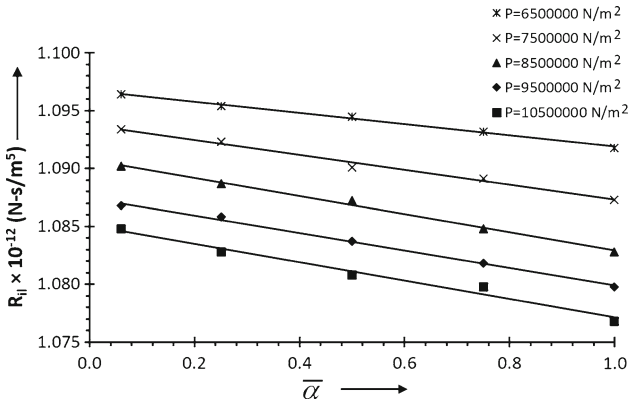

Fig. 5 Internal leakage resistance characteristics of the hydraulic motor

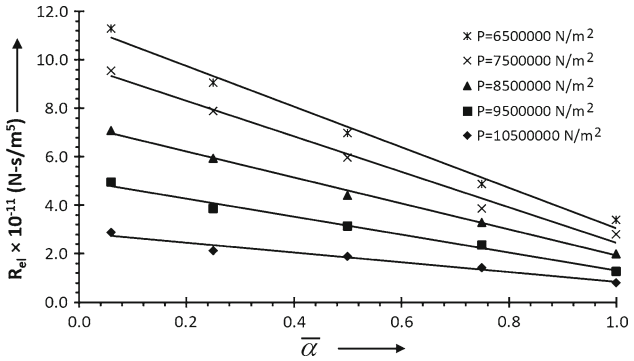

Fig. 6 External leakage resistance characteristics of the hydraulic motor

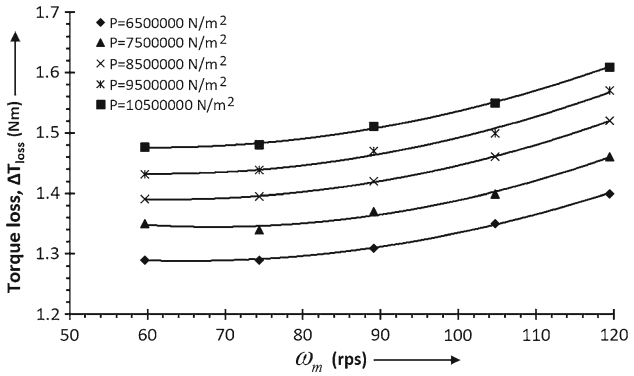

Fig. 7 Torque loss characteristics of the hydraulic motor

where ΔT_{loss} is the torque loss of the each motor and it is determined by the test data.

The variation of torque loss with ω_{m} shown in Fig. 7 is expressed by the following empirical equation:

$$\Delta T_{\text{loss}} = \left(4 \times 10^{-5}\right) \omega_{\text{m}}^2 + \left(2 \times 10^{-10} P - 0.0065\right) \omega_{\text{m}} + \left(4 \times 10^{-8} P + 1.2355\right) \tag{25}$$

Substituting this result into Eq. (24) gives the output torque on the each motor shaft:

$$T_{\text{m}} = D_{\text{m}} P - \left[\left(4 \times 10^{-5}\right) \omega_{\text{m}}^2 + \left(2 \times 10^{-10} P - 0.0065\right) \omega_{\text{m}} + \left(4 \times 10^{-8} P + 1.2355\right)\right] \tag{26}$$

Equations (17), (23) and (26) are non-dimensionalized using the following relations:

$$\omega_{\text{m}} = \overline{\omega_{\text{m}}} \frac{D_{\text{pmax}} \omega_{\text{p}}}{2 D_{\text{m}}}, \quad T_{\text{m}} = \overline{T_{\text{m}}} D_{\text{m}} P_{\text{max}},$$
$$Q_{\text{p}} = \overline{Q_{\text{p}}} D_{\text{pmax}} \omega_{\text{p}}, \quad P = \overline{P} P_{\text{max}} \tag{27}$$

Substituting them in Eq. (17), the motor efficiency is given by:

$$\eta_{\text{m}} = \frac{\overline{T_{\text{m}}}\,\overline{\omega_{\text{m}}}}{\overline{P}\,\overline{Q_{\text{p}}}} \tag{28}$$

Similarly, using Eq. (27) in Eq. (23), the non-dimensional shaft speed for the motor is:

$$\overline{\omega_{\text{m}}} = \overline{\alpha} - K_0 \overline{P} \left[\frac{1}{\left(K_1 \overline{\alpha}^2 - K_3 \overline{\alpha} - K_5\right) \overline{P} - K_2 \overline{\alpha}^2 + K_4 \overline{\alpha} + K_6} + \frac{2}{\left(-K_7 \overline{\alpha} - K_9\right) \overline{P} - K_8 \overline{\alpha} + K_{10}} + \frac{2}{\left(K_{11} \overline{\alpha} - K_{13}\right) \overline{P} - K_{12} \overline{\alpha} + K_{14}} \right] \tag{29}$$

where

$$K_7 = 8 \times 10^2 P_{\text{max}}, \quad K_8 = 0.0006 \times 10^{12},$$
$$K_9 = 3 \times 10^3 P_{\text{max}}, \quad K_{10} = 1.1155 \times 10^{12},$$
$$K_{11} = 2 \times 10^5 P_{\text{max}}, \quad K_{12} = 19.182 \times 10^{11},$$
$$K_{13} = 2 \times 10^5 P_{\text{max}}, \quad K_{14} = 25.836 \times 10^{11} \tag{30}$$

Finally, using Eq. (27) in Eq. (26), the non-dimensional torque on the output shaft of the each motor is expressed as:

$$\overline{T_{\text{m}}} = \overline{P} - B_4 \overline{\omega_{\text{m}}}^2 + \left(-B_5 \overline{P} + B_6\right) \overline{\omega_{\text{m}}} - B_7 \overline{P} - B_8 \tag{31}$$

where

$$B_4 = 10^{-5} \left(\frac{D_{\text{pmax}}^2 \omega_{\text{p}}^2}{D_{\text{m}}^3 P_{\text{max}}} \right), \quad B_5 = 10^{-10} \left(\frac{D_{\text{pmax}} \omega_{\text{p}}}{D_{\text{m}}^2} \right),$$
$$B_6 = 0.0065 \left(\frac{D_{\text{pmax}} \omega_p}{2 D_{\text{m}}^2 P_{\text{max}}} \right), \quad B_7 = \frac{4 \times 10^{-8}}{D_{\text{m}}}$$
$$\text{and } B_8 = \frac{1.2355}{D_{\text{m}} P_{\text{max}}} \tag{32}$$

After obtaining the values of the coefficients given in Eqs. (30) and (32), the efficiency map of the hydraulic motor is generated from the simultaneous solutions of Eqs. (28), (29) and (31). This is discussed in Sect. 4.

3.3 Gear Unit Analysis

The efficiency of the gear unit is expressed as:

$$\eta_g = \frac{T_d \omega_d}{2 T_m \omega_m} \tag{33}$$

The output torque on the drive shaft is:

$$T_d = 20 T_m \tag{34}$$

The angular velocity of the drive shaft is:

$$\omega_d = \frac{\omega_m}{10} \tag{35}$$

Equations (33), (34) and (35) are non-dimensionalized using the following relations:

$$T_d = \overline{T_d}\,(20 D_m P_{max}), \quad \omega_d = \overline{\omega_d}\frac{D_{pmax}\omega_p}{20 D_m},$$
$$\omega_m = \overline{\omega_m}\frac{D_{pmax}\omega_p}{2 D_m}, \quad T_m = \overline{T_m} D_m P_{max} \tag{36}$$

Substituting them in Eq. (33), the gear unit efficiency is given by:

$$\eta_g = \frac{\overline{T_d}\,\overline{\omega_d}}{\overline{T_m}\,\overline{\omega_m}} \tag{37}$$

Similarly, using Eq. (36) in Eq. (34), the non-dimensional output torque on the drive shaft is:

$$\overline{T_d} = \overline{T_m} \tag{38}$$

Finally, using Eq. (36) in Eq. (35), the non-dimensional angular velocity of the drive shaft is:

$$\overline{\omega_d} = \overline{\omega_m}. \tag{39}$$

3.4 HST Drive Analysis

The overall efficiency of the HST drive has been presented in Eq. (1) of this article. Using Eqs. (11) and (36) in Eq. (1), the overall efficiency of the drive is given as:

$$\eta_o = \frac{\overline{T_d}\,\overline{\omega_d}}{\overline{T_p}} \tag{40}$$

Table 1 Parametric values of the hydrostatic components

Symbol	Value
D_{pmax}	$4.46 \times 10^{-6}\ m^3/rad$
D_m	$2.55 \times 10^{-6}\ m^3/rad$
P_{max}	$120 \times 10^5\ N/m^2$
ω_p	150.8 rad/s

where $\overline{T_p}$, $\overline{T_d}$ and $\overline{\omega_d}$ are given by Eqs. (15), (38) and (39), respectively. These three equations, with Eq. (40) create four nonlinear independent equations that must be simultaneously solved in order to map the overall efficiency of the HST drive.

4 Results and Discussion

In order to create the efficiency maps of the pump, hydraulic motor and the HST drive, the coefficients given in Eqs. (14), (16), (30) and (32) are determined from the parametric values of the hydrostatic components given in Table 1. The values of these coefficients are given in Tables 2 and 3.

In developing the efficiency map of the pump, the three independent Eqs. (12), (13) and (15) are solved simultaneously; they are nonlinear in nature and have five unknown parameters ($\overline{\alpha}$, $\overline{P}$, $\overline{Q_p}$, $\overline{T_p}$ and η_p). Assuming that the values of two parameters ($\overline{\alpha}$, $\overline{P}$) are known out of the five unknown parameters in Eqs. (12), (13) and (15), simultaneously solving these equations using Newton–Raphson numerical method, the values of the other three unknown parameters ($\overline{Q_p}$, $\overline{T_p}$ and η_p) are determined. Using them, the efficiency map of the pump is created. Likewise solving Eqs. (28), (29) and (31) simultaneously, the efficiency map for the hydraulic motor is developed. Similarly, the efficiency map of the overall HST drive is made from Eqs. (15), (38), (39) and (40). The efficiency maps of the pump, hydraulic motor and the HST drive are given in Figs. 8, 9 and 10, respectively.

Figure 8 illustrates that the pump's efficiency is independent of pump flow at low pressures, whereas it is independent of fluid pressure at low flow rates. The near-vertical and horizontal lines of the efficiency in the regions of low pressure and low flow rate indicate the same. It may be noted that at maximum operating pressure, the maximum efficiency of the pump may not be obtained. The reasonable efficiency zone of the pump is obtained in medium to high pressure range and at high flow rates as it is appears in Fig. 8. The maximum efficiency of the hydrostatic pump is found to be 94%.

Figure 9 illustrates that the hydraulic motor's efficiency is independent of output torque at low motor shaft speeds, whereas it is independent of motor shaft speed at low output torque. The near-vertical and horizontal lines of the efficiency in the regions of low output torque and low motor shaft

Table 2 Pump coefficients in Eqs. (14) and (16)

Symbol	Value	Symbol	Value	Symbol	Value
K_0	1.78×10^{10}	K_1	1.2×10^{11}	K_2	0.2318×10^{11}
K_3	8.4×10^{10}	K_4	1.2568×10^{11}	K_5	3.6×10^{11}
K_6	7.2137×10^{11}	B_0	0.02705	B_1	0.0244
B_2	0.0338	B_3	3.725×10^{-3}		

Table 3 Hydraulic motor coefficients in Eqs. (30) and (32)

Symbol	Value	Symbol	Value	Symbol	Value
K_7	9.6×10^{9}	K_8	0.0006×10^{12}	K_9	3.6×10^{10}
K_{10}	1.1155×10^{12}	K_{11}	2.4×10^{12}	K_{12}	19.182×10^{11}
K_{13}	2.4×10^{12}	K_{14}	25.836×10^{11}	B_4	0.022734
B_5	0.01034	B_6	0.02801	B_7	0.01569
B_8	0.04038				

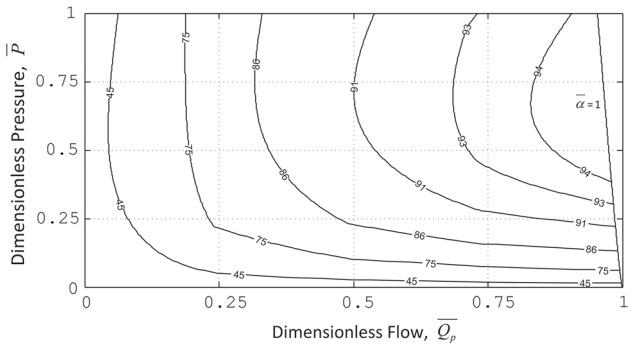

Fig. 8 A typical efficiency map for the hydraulic pump

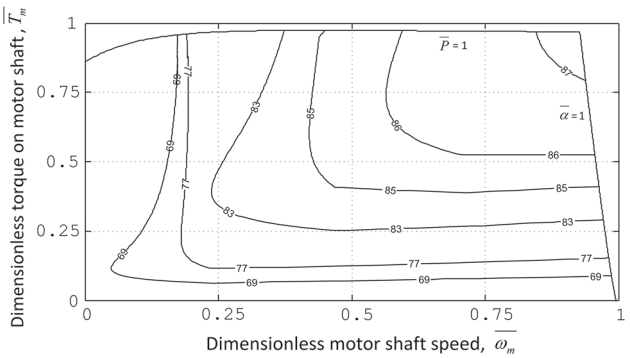

Fig. 9 A typical efficiency map for the hydraulic motor

speed indicate the same. The reasonable efficiency zone of the hydraulic motor is obtained in higher output torque and speed as it is appears in Fig. 9. The maximum efficiency of the hydraulic motor is found to be 87%.

Figure 10 gives the efficiency characteristics of an HST drive considered in the present study. Because of the limitation of the operating pressure, the characteristics of the drive show similar nature that have been discussed for the hydraulic motor. Within the maximum operating pressure

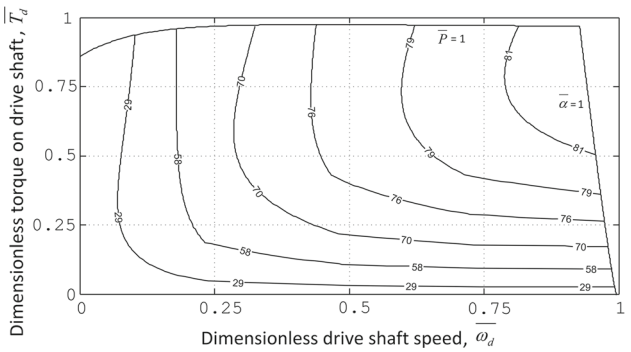

Fig. 10 A typical efficiency map for the HST drive

and swash plate angle of the pump, such characteristics are drawn. The characteristics indicate that the efficiency of the drive is independent of the output torque at low shaft speed, whereas it is independent of the shaft speed at low output torque. The efficiency of the HST drive basically depends upon the efficiency of the pump and the hydraulic motor. It is apparent from the visual examination of Fig. 10 which is more or less an overlay of Figs. 8 and 9. As discussed in Fig. 9, the maximum efficiency of the hydraulic motor is obtained at higher torque and speed range. However, due to the effect of the pump efficiency (Fig. 8), the maximum efficiency of the drive is observed for medium to high torque and high speed range. The maximum efficiency of the HST drive is found to be 81%.

5 Load Characteristics in Drilling

The torque required to rotate the drill bit is expressed by the following empirical relation [8–10]:

$$T_{\mathrm{d}} = \frac{1.32 \times 10^{-7} \times k \times D^{3.4} \times E^{0.5} \times S^2 \times R}{\omega_{\mathrm{d}}} \tag{41}$$

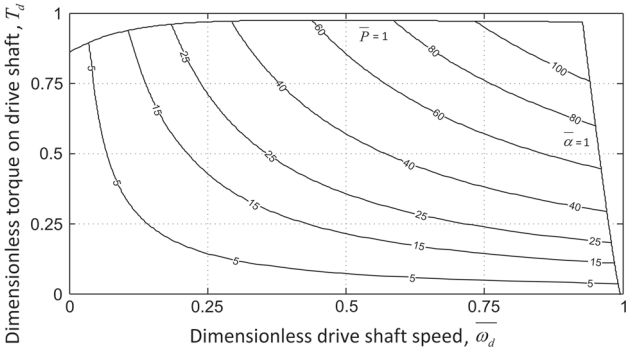

Fig. 11 Characteristics of the penetration rate

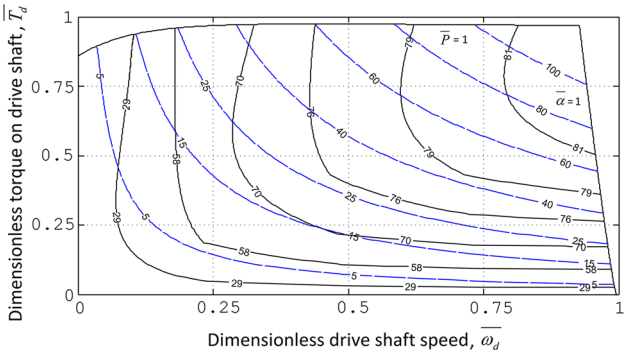

Fig. 12 Performance of the HST drive with the variation of penetration rate

where T_d is the required torque to rotate the drill bit (Nm), R is the penetration rate (m/h), E is the feed force (kg), ω_d is the drill bit rotary speed (rad/s), S is the rock compressive strength (MPa), D is the diameter of the drill bit (mm) and k is the constant related to the properties of the rock. Values for the constant k lie between 14×10^{-5} and 4×10^{-5} and it depends upon the drillability of the rock. For harder rock, lower value is considered, whereas for the soft rock higher value is used.

For a constant feed force ($E = 13{,}600$ kg) and diameter of a drill bit ($D = 174$ mm), the drill performance for the soft rock-like coal ($S = 30$ MPa) largely depends upon its rotational speed (ω_d) and drill torque (T_d). Substituting the above values in Eq. (41), the drill penetration rate is expressed as:

$$R = \frac{T_\mathrm{d}\omega_\mathrm{d}}{57.47} \tag{42}$$

Using Eq. (36) in Eq. (42), the drill penetration rate is:

$$R = c\overline{T_\mathrm{d}}\,\overline{\omega_\mathrm{d}} \tag{43}$$

where

$$c = \frac{D_\mathrm{pmax}\omega_\mathrm{p}P_\mathrm{max}}{57.47} = 140.44.$$

With respect to the penetration rate that varies from 5 to 100 m/h, the torque speed characteristics for the rotary head of drill machine for cutting coal is shown in Fig. 11 which shows that the higher penetration rate is obtained at higher torque and speed range, whereas it decreases at low speed and high torque range as well as at high speed and low torque range.

The effect of drive efficiency on penetration rate is shown in Fig. 12 which is plotted by overlaying Figs. 10 and 11. It indicates that at higher torque and higher speed range with increase in the drive efficiency the penetration rate also increases. Usually, for drilling coal the penetration rate varies from 50 to 80 m/h. To achieve higher penetration rate, the higher torque and speed is needed which may be obtained from high-capacity plunger pump that exhibits fairly good efficiency at high operating pressure.

6 Conclusion

In the present work, the studies have been made regarding the efficiency map of the HST drive for the rotary head of drill machine using two high-speed low-torque hydraulic motors along with a gear reducer unit. In this respect, the system model is made which is validated experimentally. While modelling, the various losses of the HST drive are taken into account by the resistive elements. They were identified experimentally and found to be nonlinear in nature. The results are presented in non-dimensional form, from where selection of any size of the HST drive can be made.

The following conclusions are drawn from the studies conducted in this article:

1. In medium to high pressure range and at high flow rates, the maximum efficiency of the variable displacement axial piston pump is found to be 94%.
2. At higher output torque and speed, the maximum efficiency of the fixed displacement bent axis hydraulic motor is found to be 87%.
3. The maximum efficiency of the HST drive is observed near medium to high torque and high speed range which is above 81%.
4. The characteristics of the HST drive indicate that the efficiency of the drive is independent of the output torque at low shaft speed, whereas it is independent of the shaft speed at low output torque.

5. At higher torque and higher speed range with increase in the drive efficiency, the penetration rate also increases.

The idea for generating the efficiency map for the mining equipment proposed in this article would have considerable value to study the control aspect of the drive. It may be useful for the initial design of the machine from where one can get an economical solution for the selection of hydrostatic components for similar applications. The viability of the HST drive discussed in this article depends upon the efficiency gain throughout its working range. Based on that, the system designer may take decision regarding the use of such drive for continuously variable transmission application. From the torque loss and the leakage characteristics of the pump and the hydraulic motor shown in Figs. 3, 4, 5, 6 and 7, suitable control scheme may be formulated for varying the pump displacement ratio ($\overline{\alpha}$) to obtain higher efficiency of the drive. This may be a future scope of work.

Appendix 1

Experimental Test Set-Up

The detailed experimental test set-up for evaluating the performance of the HST drive discussed in Sect. 2 is shown in Fig. 13. Table 4 gives the summary of the major components used in the test set-up.

In the test set-up, a variable displacement pump (2) rotated at a constant speed by a prime mover (1) supplies pressurized fluid to the hydraulic motors (5) that in turn drive the load. Both the motors (5) are connected through a gear reducer unit (6). The output shaft of which drives a variable displacement pump (7) in the loading circuit. The loading pump (7) supplies flow to the proportional pressure relief valve (8). By adjusting the set pressure of the valve (8) or swash plate angle of the pump (7), the load on the motors (5) is varied. Such adjustments are made through command signal given

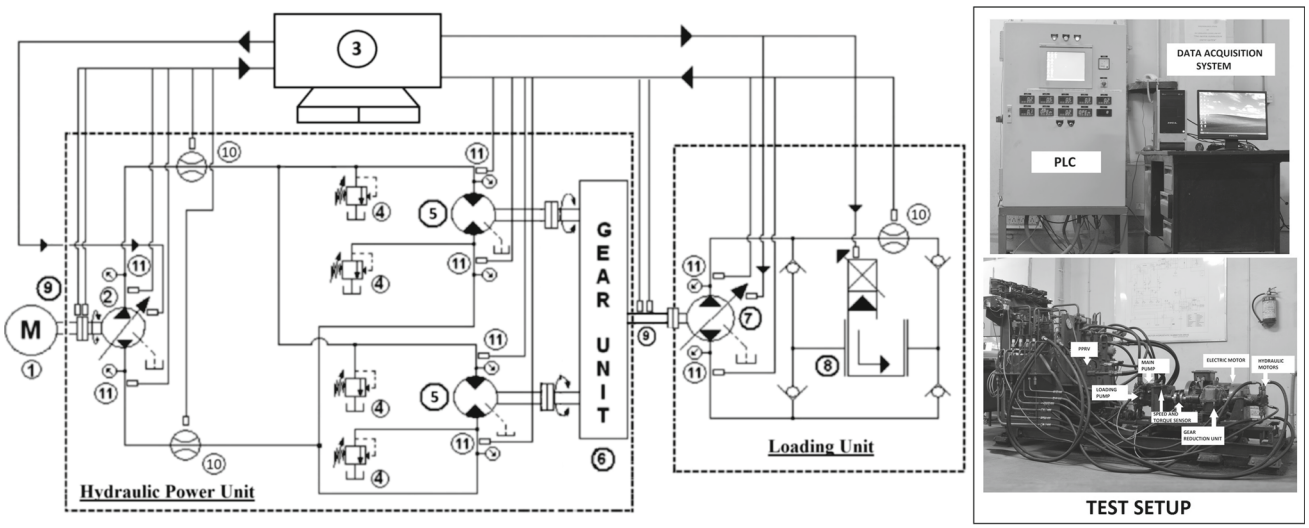

Fig. 13 Experimental test set-up of the HST drive. 1. Electric motor, 2. variable displacement axial piston pump, 3. data acquisition system, 4. pressure relief valve, 5. bent axis hydraulic motor, 6. gear reducer unit, 7. loading pump, 8. proportional pressure relief valve, 9. speed and torque sensor, 10. flow sensor, 11. pressure sensor

Table 4 Summary of the major components used in the test set-up of the HST drive

S. No.	Items	Make/model	Descriptions
1.	Variable displacement axial piston pump [11]	Bosch Rexroth Germany (A4VG28EP2DM1/3X–RPZC10F02D)	$D_P = 28$ cc/rev
2.	Bent axis motor [12]	Bosch Rexroth Germany (A2FM16/61W-VBB030)	$D_m = 16$ cc/rev
3.	Gear reducer unit [13]	New Allenberry Works India, CSB140	Gear ratio = 1:10
4.	Flow sensor	Rockwin Flowmeter India Pvt. Ltd. (TFM 1015)	Turbine flow sensor, 0–60 LPM, ± 0.5% (accuracy)
5.	Pressure sensor	Wika Germany (S-10)	0–200 bar, 0.25% (accuracy)
6.	Speed sensor	Monarch Instrument USA (ROS-W)	Non-contact, 0–2500 rpm, ± 1 RPM or 0.005% of reading
7.	Torque sensor	Honeywell Sensotec USA (2100A series)	1000 Nm, less than ± 0.05% full-scale torque

from control panel. The pressure, flow, speed and torque are measured by the respective sensors, and they are recorded in data acquisition system (3). During experiment, the oil temperature was maintained at 50 $\pm$ 2 °C using suitable oil cooler to keep the viscosity of the fluid almost constant with reasonable accuracy.

References

1. Manring, N.D.: Mapping the efficiency for a hydrostatic transmission. J. Dyn. Syst. Meas. Control **138**(3), 031004 (2016)
2. Manring, N.D.: Efficiency mapping for a linear hydraulic-actuator. J. Dyn. Syst. Meas. Control **135**(6), 064505 (2013)
3. Wang, A.; Yue, B.; Jiang, K.; Li, X.: Non-linear improvement on hydraulic pump and motor models based on parameter optimization algorithms. In: International Conference on Artificial Intelligence and Computational Intelligence (pp. 16–23). Springer, Berlin (2010)
4. Vanwalleghem, B.; Dousy, C.; Pinte, G.; Vanseveren, B.: Optimization of the efficiency of hydrostatic drives. In: 8th International Fluid Power Conference, Dresden (2012)
5. Vardhan, A.; Dasgupta, K.; Kumar, N.: Comparison of the steady-state performance of hydrostatic drives used in the rotary head of the drill machine. J. Braz. Soc. Mech. Sci. Eng. (2017). https://doi.org/10.1007/s40430-017-0803-z
6. Comellas, M.; Pijuan, J.; Potau, X.; Nogues, M.; Roca, J.: Analysis of a hydrostatic transmission driveline for its use in off-road multiple axle vehicles. J. Terramech. **49**, 245–254 (2012)
7. Product catalogue of operation & maintenance manual C-650, Revathi Equipment Limited Coimbatore, India
8. Li, Z.; Itakura, K.I.: Drilling processes using drag bits and its application. J. Civ. Eng. Archit. **6**, 715 (2012)
9. Karasawa, H.; Ohno, T.; Miyazaki, K.; Eko, A.: Experimental results on the effect of bit wear on torque response. Int. J. Rock Mech. Min. Sci. **84**, 1–9 (2016)
10. Jimeno, E.L.; Jimino, C.L.; Carcedo, A.: Drilling and Blasting of Rocks. CRC Press, Boca Raton (1995)
11. Product catalogue of the variable displacement pump RA 92003-A/06.09, Bosch Rexroth India Ltd
12. Product catalogue of the bent axis piston motor RE 91 001/09.00, Bosch Rexroth India Ltd
13. Product catalogue of standard gear unit modular system CSB140, New Allenberry Works, India